HHS Public Access

Author manuscript

Cell Rep. Author manuscript; available in PMC 2016 October 21.

Published in final edited form as:

Cell Rep. 2016 September 20; 16(12): 3195–3207. doi:10.1016/j.celrep.2016.08.050.

Multivalent chromatin engagement and inter-domain crosstalk regulate MORC3 ATPase

Forest H. Andrews[1,*], **Qiong Tong**[1,*,#], **Kelly D. Sullivan**[1,4], **Evan M. Cornett**[2], **Yi Zhang**[1], **Muzaffar Ali**[1], **JaeWoo Ahn**[1], **Ahway Pandey**[1,4], **Angela H. Guo**[3], **Brian D. Strahl**[3], **James C. Costello**[1], **Joaquin M. Espinosa**[1,4], **Scott B. Rothbart**[2], and **Tatiana G. Kutateladze**[1]

[1]Department of Pharmacology, University of Colorado School of Medicine, Aurora, CO 80045, USA

[2]Center for Epigenetics, Van Andel Research Institute, Grand Rapids, MI 49503, USA

[3]Department of Biochemistry & Biophysics, The University of North Carolina School of Medicine, Chapel Hill, NC 27599, USA

[4]Linda Crnic Institute for Down Syndrome, University of Colorado School of Medicine, Aurora, Colorado 80045, USA

Abstract

MORC3 is linked to inflammatory myopathies and cancer, however the precise role of MORC3 in normal cell physiology and disease remains poorly understood. Here, we present detailed genetic, biochemical, and structural analyses of MORC3. We demonstrate that MORC3 is significantly upregulated in Down syndrome, and that genetic abnormalities in MORC3 are associated with cancer. The CW domain of MORC3 binds to the methylated histone H3K4 tail, and this interaction is essential for the recruitment of MORC3 to chromatin and accumulation in nuclear bodies. We show that MORC3 possesses intrinsic ATPase activity that requires DNA however is negatively regulated by CW, which interacts with the ATPase domain. Natively linked CW

Correspondence: Tatiana G. Kutateladze, tatiana.kutateladze@ucdenver.edu.

[#]Current address: Wuhan Institute of Physics and Mathematics Chinese Academy of Sciences, Wuhan, China

[*]Equal contribution

SUPPLEMENTAL INFORMATION

Supplemental Information includes Extended Experimental Procedures, six figures and three tables and can be found with this article online at XXX.

ACCESSION NUMBERS

Atomic coordinates for the structures of the MORC3 CW domain in complex with H3K4me3, H3K4me1, and H3K4me0 peptides have been deposited in Protein Data Bank under accession codes 5SVX, 5SVY, and 5SVI. RNA-seq data has been deposited in the Gene Expression Omnibus under accession numbers GSE78942 and GSE84531.

Author contributions

F.H.A., Q.T., K.D.S., E.M.C., Y.Z., M.A., J.A., A.P., A.H.G., J.C.C. and S.B.R. performed experiments and together with B.D.S., J.M.E. and T.G.K. analyzed the data. F.H.A., K.D.S., S.B.R. and T.G.K. wrote the manuscript with input from all authors. Lead contact: T.G.K.

While this manuscript was in final preparation, the Liu et al. study appeared online reporting the structural mechanism for binding of MORC3 CW to H3K4me3 (Liu et al., 2016). The structures of the MORC3 CW-H3K4me3 complexes reported in this study and by Liu et al are very similar.

impedes binding of the ATPase domain to DNA, resulting in a decrease in the DNA-stimulated enzymatic activity. Collectively, our studies provide a molecular framework detailing newly identified functions of MORC3 and suggest that its modulation may contribute to human disease.

eTOC

MORC3 is upregulated in Down syndrome and is linked to cancer. Using genetic, biochemical, and structural analyses, Andrews et al show that MORC3 CW domain associates with methylated histone H3, and negatively regulates MORC3 DNA-dependent ATPase activity by binding to MORC3 ATPase domain.

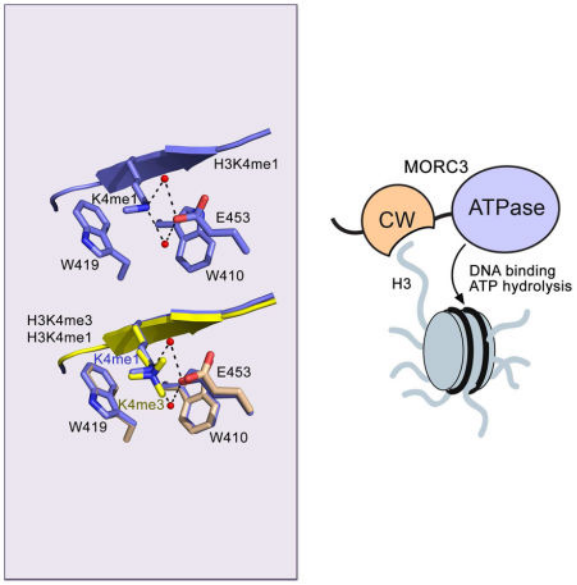

Introduction

Microrchidia 3 (MORC3) is a member of the Morc family of four proteins evolutionarily conserved throughout the eukaryotic kingdom. MORC3, also called nuclear matrix protein 2 (NXP2), was originally identified as a nuclear matrix-associated protein with RNA-binding activity (Kimura et al., 2002). It is one of the most common auto-antigens present in inflammatory myopathies, with one fourth of juvenile dermatomyositis (DM) patients being found positive for anti-MORC3 antibodies (Gunawardena et al., 2009). Recent clinical studies reveal elevated MORC3 expression in leukocytes following anti-cancer chemotherapy (Gonzalez-Fernandez et al., 2012). MORC3 localizes to promyelocytic leukemia nuclear bodies (PML-NBs), where it regulates p53 activity essential for cellular senescence in human and mouse fibroblasts (Mimura et al., 2010; Takahashi et al., 2007). Accumulating evidence suggests a role of MORC3 in transcription, as it promotes gene silencing when bound to SUMO-2 (Rosendorff et al., 2006).

MORC3 is a large, 939-residue multi-modular protein. It contains an N-terminal gyrase, Hsp90, histidine kinase, and MutL (GHKL)-type ATPase domain, which is conserved in other human MORC family members (MORC1, MORC2 and MORC4) and is also present

in a diverse array of chromatin-modified enzymes and chaperones (reviewed in (Dutta and Inouye, 2000; Li et al., 2013)). Although the catalytic activity of MORC3 has not been established, the ATP-hydrolyzing function of orthologous and homologous Morc proteins was found to be essential for heterochromatin condensation and gene silencing in *Arabidopsis thaliana* and for chromatin remodeling in response to DNA damage in mammalian cells (Li et al., 2013; Moissiard et al., 2012; Pastor et al., 2014). The ATPase domain in MORC3 is followed by a CW-type zinc finger and a C-terminal coiled-coil region. The MORC3 CW domain has been shown to interact with histone H3 peptides (Li et al., 2012; Liu et al., 2016), however the functional significance of this interaction remains unclear. The biological role of the coiled-coil region is unknown, though it may mediate protein dimerization.

Recent reports have demonstrated that MORC3 is misregulated in the brain of a Down syndrome mouse model (Ling et al., 2014) and anti-MORC3 antibodies are found in most patients with cancer-associated dermatomyositis (Fiorentino et al., 2013), yet the precise role of MORC3 in normal cellular processes and in disease has not been determined. Here, we present detailed genetic, biochemical, and structural analyses of MORC3. We report on histone H3K4me- and DNA-binding functions of MORC3, inter-domain crosstalk, and intrinsic catalytic activity of this ATPase. Our mechanistic and mutagenesis studies reveal an intricate multivalent engagement of MORC3 with chromatin and regulation of the ATPase activity by DNA and CW and suggest a possible link between the impaired MORC3 histone-binding activity and disease.

Results and Discussion

MORC3 is markedly upregulated in Down syndrome

Because the *MORC3* gene is encoded on chromosome 21 (chr21), trisomy of which causes Down syndrome (DS), the most common chromosomal abnormality in humans, we examined whether *MORC3* contributes to the disease pathology. We first analyzed and compared expression of *MORC3* and two other family members, *MORC2* and *MORC4*, which are located on chr22 and chrX, respectively, using the Genotype-Tissue Expression (GTEx) portal. We found that all three genes are expressed ubiquitously across tissues and to similar levels (Fig. 1a). To determine whether *MORC3* is subject to inter-individual and tissue-specific variation, we next performed RNA sequencing (RNA-seq) on a panel of 12 age- and gender-matched euploid (D21) and T21 fibroblasts and measured *MORC3*, *MORC2* and *MORC4* expression levels. We found that *MORC3* is substantially upregulated in T21 cells compared to D21 cells, and this discernible upregulation is conserved across different individuals (Fig. 1b). In contrast, *MORC2* and *MORC4* expression levels remained unchanged in T21 and D21 cells.

To test whether *MORC3* upregulation is conserved in a different tissue, we carried out RNA-seq on a panel of six age-matched female D21 and T21 lymphoblastoid cells. Like in fibroblasts, *MORC3* (but not *MORC2*) was notably upregulated in T21 lymphoblastoid cells relative to D21 cells (Fig. 1c). *MORC4* was also strongly upregulated in T21 lymphoblastoid cells, however this upregulation appeared to be unique to these cell lines and potentially confounded by the near absolute lack of *MORC4* expression in D21 cells. Finally, to

examine *MORC3* expression levels in naïve patient samples, we isolated monocytes and T cells from 17 individuals (10 T21 and 7D21), extracted RNA and performed RNA-seq. Analysis of the RNA-seq data revealed consistent upregulation of *MORC3*, but not *MORC2* or *MORC4*, in individuals with T21 (Fig. 1d). Furthermore, the observed upregulation level of *MORC3* was equal to or greater than that of genes known to contribute to DS pathology, including *RCAN1, DYRK1A, APP and RUNX1*. For example, in monocytes from individuals with T21, *MORC3* is upregulated to a greater extent (1.69 fold) than *RCAN1* (1.36 fold), *DYRK1A* (1.31 fold), *APP* (1.21 fold) and *RUNX1* (0.86 fold). Together, these results demonstrate high expression level of *MORC3* in cells from individuals with DS, which is conserved across different tissue types.

To establish whether *MORC3* upregulation is conserved across species, we analyzed our RNA-seq datasets against a published dataset of gene expression in brains of a mouse Ts1Cje model of DS. The Ts1Cje model has a partial triplication of the region of mouse chromosome 16 that is syntenic to human chr21. Strikingly, while relatively few genes are consistently upregulated in the five datasets, *MORC3* is found among the 15 that are (Fig. 1e). Such conservation of *MORC3* upregulation among individuals, tissues, and even species, suggests that *MORC3* could be part of a core signaling cascade consistently deregulated by trisomy 21.

Genetic abnormalities in *MORC3* are associated with cancer

A subset of DM patients has been reported to be at increased risk of malignancies at the time of DM diagnosis (Fiorentino et al., 2013; Madan et al., 2009). Since most patients with cancer-associated DM present antibodies to MORC3 (Fiorentino et al., 2013), we sought to characterize a possible link between MORC3 and cancer. We performed a survey of genetic alterations in *MORC3* across human cancers collected in The Cancer Genome Atlas (TCGA). *MORC3* is altered (mutation, amplification, or deletion) in multiple cancers, most frequently in bladder, uterine, stomach and lung cancers, as well as diffuse large B-cell lymphomas (Fig. S1a). We further explored the impact of these alterations on patient outcomes and found that patients with amplifications of *MORC3* showed significantly poorer overall survival in sarcoma ($p=0.002$, log-rank test), acute myeloid leukemia ($p=0.004$, log-rank test), stomach adenocarcinoma ($p=0.013$, log-rank test), breast invasive carcinoma ($p=0.034$, log-rank test), and uterine corpus endometrial carcinoma ($p=0.036$, log-rank test) (Fig. S1b). We note that a possible association of MORC3 antibody-positive idiopathic inflammatory myopathies and cancer has also been suggested (Ichimura et al., 2012). Together, the genetic abnormalities found in DS, DM and cancer patients point to a physiological importance of MORC3, yet our knowledge of its function at the molecular level is very limited.

Binding of MORC3-CW to the histone H3 tail is modulated by PTMs

In an effort to better understand the mechanism of action of MORC3, we carried out biochemical and structural analyses of its functional modules, the CW domain and the ATPase domain (Fig. 2a). While the CW domain of MORC3 was shown to associate with the histone H3 tail (Li et al., 2012), its preference for and regulation by posttranslational modifications (PTMs) have not been characterized. To determine the specific binding partner

and assess the effect of PTMs on binding activity of MORC3-CW, we tested the CW domain in a high-throughput histone peptide microarray (Fig. 2b–d). A GST-fusion of CW was incubated with a library of ~200 synthetic histone peptides containing known single and combinatorial PTMs (lysine acetylation, lysine and arginine methylation, arginine citrullination, and serine/threonine phosphorylation) found in the core and variant histone proteins (Tables S1 and S2). Microarray results showed that the MORC3 CW domain recognizes N-terminal histone H3 peptides but does not recognize H2A, H2B or H4 peptides (Fig. 2d). The effect of single modifications on CW binding varied, with methylation of H3K4 enhancing this interaction, and methylation or citrullination of H3R2, phosphorylation of H3T3 and H3T6, and acetylation of H3K4 reducing it. Interestingly, the negative effect of PTMs was essentially annulled when K4me3 was present on the same peptide, suggesting that the MORC3 CW domain is capable of binding to H3K4me3 regardless of the presence of neighboring marks.

To assess the extent of enhancement observed in the CW binding to H3K4me, we produced ^{15}N-labeled MORC3-CW and examined it in ^{1}H,^{15}N heteronuclear single quantum coherence (HSQC) titration experiments (Fig. 2e). Addition of the H3K4me3 peptide (aa 1–12 of H3) induced large chemical shift changes in MORC3-CW, indicating direct interaction. Throughout titration of the peptide, a number of crosspeaks corresponding to the free state of the protein disappeared, and simultaneously, another set of resonances, corresponding to the bound state, appeared. This pattern of chemical shift changes indicates tight binding in a slow exchange regime on the NMR time scale. Titration of the unmodified H3 peptide led to an almost identical pattern of resonance changes, and the slow exchange regime again pointed to a strong interaction and binding affinity in a low micromolar range. In agreement, dissociation constants (K_ds) for the complexes of MORC3-CW with the H3K4me3, H3K4me2, H3K4me1 and H3K4me0 peptides were found to be ~0.64, 0.67, 0.74, and 6.8 μM, respectively, as measured by intrinsic tryptophan fluorescence (Fig. 2f, g). These results suggest that the MORC3 CW domain does not efficiently discriminate between the methylation states of H3K4, displaying only a slight preference for H3K4me3 species over H3K4me2 or H3K4me1. Furthermore, although its binding affinity for H3K4me0 is ~10 fold lower, it is still in the range of binding affinities exhibited by the majority of known epigenetic readers toward modified or unmodified histones (1–50 μM) (Musselman et al., 2012). These data corroborate well the results of the most recent study that reports 0.8 μM (measured by ITC) or 1.8 μM (by FP) binding affinity of the MORC3 CW domain for H3K4me3 and a ~8-fold decrease in the affinity of this domain for H3K4me0 (Liu et al., 2016).

Structural basis for the interaction of the MORC3 CW domain with H3K4me3

To elucidate the molecular mechanism for the recognition of H3K4me3, we determined the crystal structure of the MORC3 CW domain bound to an H3K4me3 peptide to a 1.56 Å resolution (Fig. 3 and Table S3). The MORC3 CW domain has a compact globular fold consisting of a double-stranded antiparallel β sheet and a 3_{10}-helical turn linked by a single zinc-binding cluster (Fig. 3a). The H3K4me3 peptide is bound in an extended conformation. It forms a third antiparallel β-strand pairing with the β1 strand of the protein. Backbone amides of the peptide residues R2, K4, and T6 form characteristic β-sheet hydrogen bonds

with the backbone amides of Gln408, Trp410 and Gln412 of the CW domain (Fig. 3a). The N-terminal amino group of the peptide residue A1 donates two hydrogen bonds to the carbonyl groups of Pro430 and Glu431, whereas the methyl group of A1 is bound in a hydrophobic pocket lined with Trp433 (Fig. 3b). The CW:H3K4me3 complex is further stabilized through an extensive set of intermolecular hydrogen bonds involving the side chains of the peptide. The Q5 amide is hydrogen bonded to Thr409, and T6 forms a polar contact with the indole nitrogen atom of Trp410. The guanidino group of R8 is restrained through the interaction with the side chain amide of Gln408 and a salt bridge with the carboxyl group of Asp424. Another hydrogen bond is formed between the amino group of K9 and the carboxyl group of Asp454, whereas T11 is hydrogen bonded to a serine residue from the vector.

The fully extended side chain of K4me3 occupies an elongated groove made of two aromatic residues and two negatively charged residues (Fig. 3a, b). The aromatic side chains of Trp410 and Trp419 are positioned orthogonally to each other, creating side-walls of the V-shaped groove, whereas Glu450 and Glu453 in the C-terminal loop of the CW domain make the groove's end-wall. The positively charged trimethylammonium group of K4 is locked through cation-π interactions with Trp410 and Trp419 and through electrostatic interactions with the negatively charged carboxylates of Glu453 and Glu450.

Negatively charged end-wall residues direct selectivity of MORC3-CW

Given that MORC3-CW is capable of tight binding to either methylated form of H3K4, we sought to obtain mechanistic insight into this behavior by determining the crystal structure of the CW domain in complex with an H3K4me1 peptide (Fig. 3d and Table S3). We found that the overall structure of the CW:H3K4me1 complex is almost identical to the structure of the CW:H3K4me3 complex (Fig. 3d). However, there is a significant difference in coordination of K4me3 and K4me1 within the binding groove that can help explain the indifference of MORC3-CW toward the K4 methylation state. Particularly, the monomethylammonium moiety is restrained via two hydrogen bonds, formed with the carboxylate of Glu453 and mediated by two highly ordered water molecules (Fig. 3e). These water molecules are absent in the H3K4me3-binding pocket; moreover, their relative spaces are occupied by the methyl groups in the trimethylammonium moiety. The two additional hydrogen bonds observed in the K4me1-binding pocket likely compensate for the energetic loss in the hydrophobic and cation-π interactions, which contribute to coordination of K4me3 to a higher degree. While we were unable to obtain the structure of the H3K4me2-bound CW domain, based on the comparative analysis, we would anticipate that the dimethylammonium moiety is stabilized through a single water-mediated hydrogen bond with Glu453. Together, the structural data suggest that the ability of the MORC3 CW domain to interact robustly with H3K4me3/me2/me1 is likely due to the ability of the end-wall residue, Glu453, to facilitate water-mediated hydrogen bonds with H3K4 in the low methylation state.

Alignment of the CW domain sequences demonstrates that the two tryptophan residues in the histone-binding site are conserved in several other CW domains, however the negatively charged end-wall residue (Glu453 in MORC3) is not conserved (Fig. 4a). For example,

Glu453 is replaced with an aromatic tryptophan residue in the CW domain of CWPW1 that associates with H3K4me3 ~2.5-, ~6- and ~14- fold tighter than it associates with H3K4me2, H3K4me1 and H3K4me0, respectively (He et al., 2010) (Fig. 4b). To further corroborate the importance of the end-wall residues in MORC3, we generated a series of Glu453 mutants and assayed their interactions with histone peptides by fluorescence spectroscopy and NMR. We found that substitution of Glu453 with a tryptophan enhances the preference of the MORC3 CW domain toward H3K4me3 (Fig. 4c, d and Fig. S2).

The two-tryptophan V-shaped groove is also observed in another reader of H3K4me, a PHD finger of JARID1A, which selects for the trimethylated mark (Wang et al., 2009). While the tryptophan residues in the histone-binding sites of JARID1A-PHD and MORC3-CW are superimposed well, the JARID1A-PHD finger's groove does not have the end-wall residues and is fully open-ended (Fig. 4e). On the other hand, a number of H3K4me3-specific PHD fingers, including ING2, contain an aromatic residue in the end-wall position (Peña et al., 2006). Intriguingly, PHD fingers use the N-terminal loop preceding the β-sheet to create the end-wall, whereas the MORC3 CW domain uses the C-terminal loop to form its end-wall (Fig. 4e).

Substitution of Glu453 in MORC3-CW with a positively charged lysine residue resulted in a 10-fold decrease in binding to H3K4me3, indicating that electrostatic repulsion between Lys453 and the positively charged trimethylammonium group of K4 impedes complex formation (Fig. 4c, d). Similarly, a decrease in binding was observed for the E453R mutant of MORC3-CW (Fig. S2). Together, our results indicate that it is the end-wall residues in the binding site of the MORC3 CW domain that account for the ability of this domain to bind either methylation state of H3K4. While the cation-π interactions involving the aromatic Trp410 and Trp419 residues favor trimethylated lysine over di- or monomethylated lysine, the negatively charged end-wall residues enhance interaction with the low methylation states by providing extra water-mediated hydrogen bonds. Additionally, increased electrostatic attraction forces with a less delocalized positive charge in the low-methylation states of lysine would further strengthen this interaction.

Tryptophan residues are necessary for binding of MORC3-CW to H3K4me3

The critical role of the histone-binding site residues was supported by mutational analysis. We generated point-mutants of MORC3-CW and tested their stability and binding to H3K4me3 using NMR and assessed the strength of these interactions by fluorescence spectroscopy and NMR (Fig. 5). We found that Trp410 and Trp419 in the Trp-groove do not contribute equally to the interaction with H3K4me3. Substitution of Trp410 with an alanine reduced the binding by two orders of magnitude, whereas replacement of Trp419 with an alanine decreased this interaction more severely, i.e. by three orders of magnitude, and the Trp419K mutant was completely impaired in binding to H3K4me3 (Fig. 5a and Fig. S3). The uneven contribution probably reflects the fact that in the complex, the K4me3 group is placed closer to Trp419 than to Trp410. The distance from the nitrogen atom in the trimethylammonium group to the Cγ atom of Trp410 is 4.9 Å; however, the corresponding distance to Trp419 is 4.2 Å, which is 0.7 Å shorter. Much like K4me3 in the MORC3-CW:H3K4me3 complex, the monomethylammonium and ammonium moieties in the

MORC3-CW:H3K4me1 and MORC3-CW:H3K4me0 complexes lie closer to Trp419, though the complex with unmodified H3 peptide crystallized as a dimer with the histone-binding site being partially in the dimeric interface, hence precluding us to carry out detailed analysis of the binding mechanism (Fig. S4). We note that concurrent mutation of both Trp residues to alanine results in an unfolding of the protein, which infers that these residues also play a role in structural stability of the CW domain. Interestingly, the CW domain of KDM1B, a demethylase that demethylates H3K4me2/me1 (Ciccone, 2009), contains both tryptophan residues (Fig. 4a), however NMR titration experiments showed that the KDM1B CW domain does not interact with the H3K4me2 peptide, suggesting that for certain CW domains the presence of two Trp residues is necessary but not sufficient for the binding (Fig. 4f).

Substitution of Asp407, Gln408 and Gln412 residues that are involved in polar contacts in some of the MORC3-CW complexes had little effect on the interaction with H3K4me3 (Fig. 5a). However, binding of the Q408A/D424A mutant was reduced ~40-fold, pointing to the important contribution of the salt bridge formed between Asp424 and H3R8 to the interaction. We also found that the first two residues of histone H3, A1 and R2, are required for the interaction of the CW domain, as no binding was detected to the peptide containing residues T3-S10 of histone H3 (Fig. 5d).

MORC3-CW interacts with the ATPase domain

Considering the close proximity of CW to the ATPase domain, which are separated by about 12 residues in MORC3, we next asked whether the two modules are in contact. We generated an isolated ATPase domain of MORC3, purified the His-tag fusion protein and titrated it into an NMR sample containing ^{15}N-labled MORC3-CW E453A (Fig. 6a and Fig. S5; we used His-tagged ATPase due to its solubility and the E453A mutant and H3K4me0 peptide to avoid slow exchange regime and thus be able to compare the patterns of resonance changes in CW). Substantial chemical shift perturbations in CW E453A and broadening and loss of signal intensities in ^{1}H,^{15}N transverse relaxation optimized spectroscopy (TROSY) experiments upon addition of His-ATPase indicated that the two domains of MORC3 form a complex (~50 kDa in size). Although the pattern of resonance changes was distinctly different from the pattern of resonance changes induced in MORC3-CW E453A by the histone H3K4me0 peptide, many amides of CW were perturbed by either ligand, suggesting that binding interfaces may partially overlap or substantial conformational changes accompany these interactions (compare upper panels in Fig. 6a). Thermodynamic parameters for the MORC3-CW E453A:His-ATPase complex, obtained from ITC measurements, revealed a 1:1 stoichiometry of the complex and a K_d of 9 μM for the isolated, i.e. unlinked domains (Fig. 6b). Clearly, this interaction should be tighter when the two domains are physically linked.

To establish the relationship between the two binding partners of CW, we titrated H3K4me0 peptide into the CW E453A:His-ATPase (1:1 molar ratio) complex and collected ^{1}H,^{15}N TROSY spectra (Fig. 6a, lower-left panel). An appearance of the crosspeaks corresponding to the CW E453A:H3K4me0 complex and simultaneous shifting of the ATPase-perturbed resonances to their positions in the apo-state of CW suggested that the histone peptide

displaces the ATPase domain from the CW domain. Reverse titration of the His-ATPase domain into the CW E453A:H3K4me0 (1:4) complex led to the disappearance of some crosspeaks due to formation of the large CW E453A:His-ATPase complex. Although at this molar ratio of the interactors, ATPase could not efficiently displace H3K4me0, small shifting of the histone-perturbed resonances toward their positions in the apo-state also suggested that the ATPase domain disrupts the CW E453A:H3K4me0 complex. Collectively, these results indicate that MORC3-CW has two binding partners – H3 and the ATPase domain, and their binding-sites are, at least in part, overlap.

MORC3 possesses ATPase activity that requires DNA

Previously, MORC2, a homologue of MORC3, was reported to have ATPase activity; however, this function in MORC3 has not been evaluated. To determine if the GHKL-type ATPase domain of MORC3 is capable of hydrolyzing ATP, we carried out an assay that couples the release of inorganic phosphate, produced by the hydrolysis of ATP to ADP, to the enzymatic conversion of 2-amino-6-mercapto-7-methylpurine ribonucleoside (MESG) by nucleoside phosphorylase (PNP). This results in a shift in the wavelength maximum absorbance from 330 nm for MESG to 360 nm for the product. Following incubation of the MORC3 His-ATPase domain with ATP, MESG and PNP, the release of inorganic phosphate was quantified by measuring an increase in the absorbance at 360 nm. As shown in Figure 6c, the His-ATPase domain of MORC3 hydrolyzed ATP with the rate of 0.47 ± 0.03 μmol min^{-1} at 22 °C. The rate of ATP hydrolysis was increased to 0.77 ± 0.06 μmol min^{-1} in the presence of 14mer dsDNA in the reaction and to 0.80 μmol min^{-1} in the presence of a mixture of mono- and di-nucleosomes. A similar ~two-fold increase in the enzymatic activity was observed at 30 °C and a ~three-fold increase was detected with a Widom 601 (147 bp) DNA. These data demonstrate that the ATPase activity is an intrinsic function of MORC3, which is enhanced in the presence of either free or chromatinized DNA.

To assess whether the ATPase domain directly binds DNA, we used electrophoretic mobility shift assays (EMSA). Increasing amounts of His-ATPase were incubated with Widom 601 DNA or reconstituted nucleosome core particles (NCPs) and the reaction mixtures were resolved on a 5% native polyacrylamide gel (Fig. 6d, e). A gradual increase in MORC3 His-ATPase concentration in the assays resulted in a shift of the DNA and/or NCP bands, indicating direct interaction of the ATPase domain with either free or nucleosomal DNA.

CW negatively regulates DNA-dependent ATPase activity

Because the CW and ATPase domains physically interact, we examined whether the CW domain modulates the ATPase activity of MORC3. We generated a MORC3 construct harboring linked ATPase and CW domains and tested it in the ATPase assay (Fig. 6c). We found that although the linked CW domain has little negative effect on the intrinsic catalytic activity of the ATPase domain, it considerably decreased the rate of hydrolysis in the presence of DNA. Modeling of the MORC3 ATPase domain structure suggests highly positively charged surface potential (data not shown), which likely allows this domain to bind negatively charged DNA. Because the CW domain, and particularly its H3-binding site, is highly negatively charged, we hypothesized that binding of CW to the ATPase domain precludes binding of the ATPase to DNA. Indeed, EMSA experiments with 601 DNA

showed that the DNA-binding function of His-ATPase-CW of MORC3 is impaired (Fig. 6f). Of note, the CW domain itself does not bind DNA, as no significant chemical shift perturbations were detected in $^{1}H,^{15}N$ HSQC spectra of ^{15}N-labeled MORC3-CW when 601 DNA was titrated in (Fig. 6g). Interestingly, addition of the H3 peptide to His-ATPase-CW led to a slight increase in the rate of hydrolysis suggesting that binding of CW to H3 could release the ATPase domain from CW and enhance its catalytic activity (Fig. 6c). Overall, these results suggest that CW negatively regulates the DNA-dependent MORC3 ATPase activity likely through hindering DNA binding of the ATPase domain (Fig. 6h).

Histone binding function is essential for the recruitment of MORC3 to chromatin and accumulation in NBs

Our findings suggest that MORC3 is capable of engaging chromatin via multivalent contacts. To determine whether the interaction of MORC3-CW with H3 is necessary to recruit MORC3 to chromatin *in vivo,* we investigated cellular localization of Flag-tagged full length MORC3 in HeLa cells using chromatin association assays (Fig. 7a). Both wild-type (WT) MORC3 and mutants carrying mutations in the CW domain that either disrupt the CW structure (C416S and C416A) or abrogate binding to the histone H3 tail (W419A) were tested. Cells were harvested by trypsinization 48 hours post transfection, and FLAG-MORC3 in biochemically separated chromatin and soluble fractions was examined by immunoblotting. Chromatin fractionation experiments revealed that WT FLAG-MORC3 purifies in the chromatin and soluble fractions, but MORC3 mutants impaired in H3 binding did not associate with chromatin and were found only in the soluble fractions. This data demonstrate that interaction with H3 is necessary and sufficient for MORC3 to retain on chromatin.

MORC3 was previously shown to concentrate in NBs (Mimura et al., 2010; Takahashi et al., 2007). To define the role of the CW domain in this function, HeLa cells were transfected with 3xFLAG-MORC3 transgenes, and 48 hours post transfection, FLAG-tagged proteins were visualized using anti-FLAG antibodies by confocal fluorescence microscopy. As shown in Figure 7b, WT FLAG-MORC3 was found localized to NBs; however, FLAG-MORC3 W419A and FLAG-MORC3 C416A mutants that are unable to bind histones diffused throughout the nucleus. Collectively, these results underscore a direct link between histone binding of MORC3 through its CW domain and the function of MORC3 as a chromatin-associated ATPase and a NB factor.

Some cancer-relevant mutations decrease binding of MORC3-CW to H3

To date, 168 cancer-relevant aberrations, including mutations, reading frame-shifts and deletions, have been identified in *MORC3*; 7 of which reside in the CW domain (Fig. S6a, cBioPortal). Particularly, MORC3-CW R420Q mutation is found in multiple cancer types, such as prostate and stomach cancers and melanoma. To determine whether the cancer-related mutations affect binding of MORC3 to H3, we generated Q408H, R420Q, D424H, P430S, D440Y, R444G and P449R mutants of MORC3-CW found in breast, prostate, cervical, stomach, melanoma, liver and lung cancers and glioblastoma and tested the corresponding ^{15}N-labeled proteins by NMR (Fig. S6). We found that while all the mutants were stable, binding of R420Q and Q408H to H3K4me3, compared to WT, was decreased

~200-fold and ~80-fold, respectively, whereas binding of D424H was slightly reduced, and P430S, D440Y, R444G and P449R were able to associate with H3K4me3 as strong as the WT protein (Fig. S6d, e).

Mapping the cancer-relevant mutations on the structure of the CW:H3K4me3 complex reveals that some of the mutated residues are positioned to either mediate a proper fold of the domain or make contacts with the histone peptide. For example, three hydrogen bonds formed between the guanidino group of Arg420 and the backbone carbonyls of Asn445, Val448 and Pro449 bridge the C-terminal loop, which contains the end-wall residues, to the core of the CW domain. Mutating Arg420 to a glutamine would result in a loss of these bonds and may subsequently yield an incorrect conformation of the C-terminal loop. Both Gln408 and Asp424 are involved in the interactions with the side chain of histone H3R8, and, as we anticipated, mutations of these residues led to a decrease in histone binding of the CW domain. Together, our structural and mutational analyses demonstrate that two of the seven cancer-relevant mutants of MORC3-CW have compromised histone-binding activity – and thus suggest a possible relationship between this function of MORC3 and the disease.

Concluding Remarks

In this work, we present comprehensive genetic, biochemical and structural analyses of MORC3. We show that *MORC3* is markedly upregulated in DS across different individuals, tissues and species, and that genetic abnormalities in *MORC3* are associated with cancer. Overexpression of *MORC3* in multiple T21 experimental systems is particularly notable as very few genes (15, Fig. 1e) display conserved changes across our datasets. Other genes in this conserved group, including *IFNAR1*, *IFNAR2* and *HMGN1*, have previously been implicated in DS pathology (Hallam and Maroun, 1998; Lane et al., 2014; Maroun et al., 2000; Sullivan et al., 2016). Although we do not yet know what exact role *MORC3* plays in DS, the consistency of its upregulation is conspicuous and merits further investigation.

At the molecular level, we determined the structural mechanism by which MORC3-CW recognizes histone H3 tail. This distinctive mechanism provides an explanation for the ability of MORC3 to robustly interact with tri-, di-, or monomethylated H3K4 species. Interestingly, MORC3-CW binds to unmodified histone H3 although ~10-fold weaker but still with the appreciable binding affinity of 6.8 μM, which is somewhat uncommon for an H3K4me-targeting reader, and a similar ~8-fold decrease in the binding affinity and a K_d of 14.6 μM have also been reported by (Liu et al., 2016). Association of readers with the N-terminus of the histone H3 tail is often mediated by methylation of H3K4 (Musselman and Kutateladze, 2011; Musselman et al., 2012). Readers that possess an aromatic cage, such as PHD fingers or double chromodomains, recognize H3K4me3 but bind much more weakly to H3K4me0. Conversely, binding of the H3K4me0-specific readers, including ADD domains and some PHD fingers, to the histone tail is substantially compromised or blocked by trimethylation of H3K4. The difference in binding affinities for H3K4me3 vs H3K4me0 can be as high as three orders of magnitude. In this context, the MORC3 CW domain represents a distinctive H3K4me-reader that utilizes its aromatic cage to affix lysine 4 irrespective of its methylation state, reverberating a H3K9me-reader, the SAWADEE domain, that does not differentiate between the methylation states and binds H3K9me3/me2/me1 with a similar

affinity of ~2 μM (Law et al., 2013). Structural analysis of the MORC3-CW complexes with trimethylated, monomethylated and unmodified H3K4 peptides reveals that this ability is due to the presence of the negatively charged residues in the end-wall position of the H3K4-binding aromatic groove of MORC3-CW. The end-wall residues augment interaction with the low methylation states by providing additional water-mediated hydrogen bonds and increasing electrostatic attraction forces. It will be essential in future studies to establish whether the ability of MORC3 to recognize H3K4me3/me2/me1 tails almost equally well and, to a lesser extent, unmodified H3 plays a role in promoting binding and/or stabilization of this ATPase at various genomic regions enriched in these marks, including active, repressed, or condensed chromatin.

We found that the ATPase and CW domains interact and that MORC3 has intrinsic ATPase activity that is enhanced by DNA. Direct linking of CW to the ATPase domain results in a decrease in ATPase stimulation by DNA, which is likely a result of CW hindering the ATPase domain from engaging with DNA. A similar autoinhibition mode through blocking DNA/RNA-binding sites of ATPase motors by chromodomains and other domains have been reported for Chd1, CHD4 and Dbp5 ATPases (Hauk and Bowman, 2011; Hauk et al., 2010; Narlikar et al., 2013; Watson et al., 2012). In the case of Chd1, a negatively charged α-helix of the double chromodomains packs between two halves of the ATPase domain, blocking binding of DNA, and this inhibition can be relieved by nucleosomes, possibly through engagement of CHD1 regions outside chromodomains (Hauk et al., 2010).

What is the mechanism for the release of the MORC3 ATPase inhibition? Although in-depth investigation is required to fully understand this mechanism, our current model suggests that the negative regulatory function of CW and inhibition of the ATPase catalytic activity could be alleviated through binding of the CW domain to histone H3. A similar control of catalytic function by a reader domain has been reported for the histone demethylase KDM5A: binding of the first (PHD1) finger of KDM5A to histone H3K4me0 tail stimulates activity of the neighboring demethylase domain (Torres et al., 2015). Another example is the *de novo* DNA methyltransferase DNMT3A that contains an ADD domain (a reader, specific for H3K4me0) next to the catalytic methyltransferase domain. Recent elegant structural study has demonstrated that DNMT3A exists in an autoinhibitory form, in which the ADD domain interacts with and impedes enzymatic function of the catalytic domain through blocking its DNA-binding activity (Guo et al., 2015). Binding of ADD to H3K4me0 (but not to H3K4me3) disrupts the ADD-catalytic domain complex, resulting in a large rearrangement of ADD with respect to the catalytic domain and stimulation of the enzymatic activity (Guo et al., 2015).

Our cell data demonstrate that binding of the CW domain to histone H3 is required for the recruitment of MORC3 to chromatin and localization to NBs. Given the high sequence similarity between MORC3 and MORC4 and the fact that the CW domains of both proteins recognize H3K4me (Liu et al., 2016), it is likely that the chromatin-binding mode and the regulatory crosstalk of the reader (CW) and the catalytic domain (ATPase) are conserved in MORC4. However, the CW domains of MORC1 and MORC2, the other two human MORC proteins, lack one of the aromatic groove residues (W410 in MORC3, Fig. 4a) and do not interact with histone H3. This inability to bind H3 suggests that the mechanisms for

chromatin engagement and regulation of MORC1 and MORC2 are distinctly different than that of MORC3. Considering that the MORC proteins are evolutionarily conserved and that deregulation of MORCs is associated with various disease states, it is imperative to elucidate and compare such mechanisms. Understanding how MORC proteins engage and modify chromatin at the molecular level could provide insight into the cellular function of this family of ATPases.

METHODS

Cell Culture and RNA-seq

Fibroblasts were obtained from the Coriell Cell Repository and cultured in DMEM with 10% FBS. Lymphoblastoids were obtained from the Nexus BioRepository and cultured in DMEM with 10% FBS. HeLa were obtained from ATCC and cultured in DMEM with 10% FBS and 1x penicillin/streptomycin. Total RNA was harvested from ~5×10^6 cells using the Qiagen RNeasy kit per manufacturer's instructions including on-column DNAse digestion. 500 ng of RNA was used to prepare sequencing libraries using the Illumina TruSeq mRNA Library Prep Kit. Libraries were sequenced with an Illumina HiSeq2000.

Statistical Analysis

Data quality control was performed using FastQC (v0.11.2). Reads were aligned to GRCh37/hg19 with Tophat2 (v2.0.13), and high quality mapped reads (MAPQ>10) were filtered with SAMtools (v0.1.19). Gene level counts used for RPKM calculation were obtained with HTSeq (v0.6.1), and differential expression was determined with DESeq2 (v. 1.6.3), as described (Sullivan et al., 2016). Briefly, read counts were modeled with a negative binomial distribution and normalized for library size using the geometric mean. Dispersions were modeled with the empirical Bayes method and fold changes calculated. Significance was calculated using a Wald test to generate p-values and multiple hypothesis correction performed using the Benjamini-Hochberg method to generate adjusted p-values.

Isolation of Monocytes and T cells by Florescence Activated Cell Sorting (FACS)

Peripheral blood was collected in EDTA vacutainer tubes from 10 T21 patients and seven D21 controls. Blood was centrifuged at 500 rcf for 15 minutes to separate plasma, buffy coat, and red blood cells (RBCs). Peripheral Blood Mononuclear Cells (PBMCs) were isolated from the buffy coat fraction by RBC lysis and 1x PBS wash according to manufacturer's instructions (BD, 555899). After RBC lysis and PBS wash, PBMCs were stained for sorts at 10–20×10^7 cells/ml then diluted to approximately 5×10^7 cells/ml in flow cytometry sorting buffer (1x PBS, 1 mM EDTA, 25 mM HEPES pH 7.0, 1% FBS). All staining was performed in flow cytometry sorting buffer with fluorochrome-conjugated antibodies for at least 15 min on ice while protected from light. Single cell suspensions were stained with CD45 (eBioscience, HI30), CD14 (Biolegend, 63D3), CD3 (Biolegend, OKT3), CD 16 (Biolegend, B73.1), CD19 (Biolegend, HIB19), CD56 (Biolegend, 5.1H11) and CD34 (Biolegend, 561) antibodies. CD45+CD14+CD19−CD3−CD56− Monocytes and CD45+CD3+CD14−CD19−CD56− T cells were FAC-sorted into (1x Dulbecco's Modified Eagle Medium (DMEM) supplemented with 4.5g/L D-Glucose, L-Glutamine, and 5% FBS)

on the MoFlo Astrios (Beckman Coulter) at the CU-SOM Cancer Center Flow Cytometry Shared Resource.

Protein expression and purification

The human MORC3 CW domain (aa 401-455 and 407-455) was cloned into a pGEX 6p-1 vector. MORC3 ATPase (aa 1-392) and ATPase-CW (aa 1-455) constructs were cloned into a pET28a vector. Unlabeled and uniformly ^{15}N-labeled proteins were expressed in Rosetta2 (DE3) pLysS in LB or minimal media supplemented with $^{15}NH_4Cl$ (and 50 μM $ZnCl_2$ for CW). Protein expression was induced with 0.5 mM IPTG for 16 h at 18 °C. The His-ATPase and His-ATPase-CW proteins were purified on Ni-NTA agarose beads (QIAGEN). The protein-bound beads were washed at least 3 times with a 10 mM HEPES pH 7.4 buffer, containing 500 mM NaCl and 20 mM imidazole, and the His-tagged proteins were eluted with a 10 mM HEPES pH 7.4 buffer, containing 300 mM NaCl and 200 mM imidazole. The GST-CW proteins were purified on glutathione Sepharose 4B beads (GE Healthcare) in 50 mM sodium phosphate pH 6.8 buffer, supplemented with 100 mM NaCl and 2 mM DTT. The GST tag was cleaved overnight at 4°C with PreScission protease. Unlabel ed proteins were further purified by size exclusion chromatography and concentrated in Millipore concentrators (Millipore). All mutants were generated by site-directed mutagenesis using the Stratagene QuikChange mutagenesis protocol, grown and purified as wild-type proteins.

NMR experiments

NMR experiments were carried out on Varian INOVA 500 MHz, 600 MHz and 900 MHz spectrometers. The ^{1}H,^{15}N HSQC and ^{1}H,^{15}N TROSY spectra of 0.1 mM uniformly ^{15}N-labelled wild type or mutated MORC3-CW (or KDM1B CW) were recorded at 298K. Experiments with the ATPase domain, shown in Figs. 6a and S5, were performed in 10 mM HEPES pH 7.4 buffer, supplemented with 100 mM NaCl, 1 mM TCEP and 7% D_2O, whereas all other NMR titration experiments with CW were performed in 50 mM phosphate pH 6.8 buffer, supplemented with 100 mM NaCl, 2 mM DTT and 7% D_2O. Binding was characterized by monitoring chemical shift changes in the proteins induced by histone peptides (synthesized by the University of Colorado Peptide Core Facility), 601 DNA, or the His-ATPase domain. The dissociation constants (K_d) were determined by a nonlinear least-squares analysis in Kaleidagraph using the equation:

$$\Delta\delta=\Delta\delta_{\max}\left(([L]+[P]+K_d)-\sqrt{([L]+[P]+K_d)^2-4[P][L]}\right)/2[P]$$

where [L] is concentration of the peptide, [P] is concentration of the protein, Δδ is the observed chemical shift change, and $\Delta\delta_{max}$ is the normalized chemical shift change at saturation. Normalized chemical shift changes were calculated using the equation $\Delta\delta=\sqrt{(\Delta\delta H)^2+(\Delta\delta N/5)^2}$, where Δδ is the change in chemical shift in parts per million (ppm).

Crystallization and structure determination of MORC3-CW in complex with H3K4me3, H3K4me1 and H3K4me0

MORC3 CW domain (residues 407-455) was concentrated to 15 mg/mL and incubated on ice with H3K4me3, H3K4me1, or H3K4me0 in a 1:1.5 molar ratio for 1 hour prior to crystallization. Crystals of the CW:H3K4me0 complex were grown using the hanging-drop diffusion method at 18 °C by mixing equal volumes of protein-peptide solution with well solution composed of 1.6 M sodium citrate (pH 6.5). Crystals of the CW:H3K4me1 and CW:H3K4me3 complexes were grown via hanging-drop by combining equal volumes of peptide-protein solution with well solution comprised of 2.5 M $(NH_4)_2SO_4$ supplemented with 0.1 M sodium acetate. X-ray diffraction data were collected from single crystals at 100 K on a beamline 4.2.2 at the Advance Light Source administrated by the Molecular Biology Consortium. Datasets were integrated and scaled using HKL2000, imosflm and SCALA. The structures were obtained by molecular replacement using the CW domain (Protein Data Bank [PDB] ID 2RR4) as a search model. The Refmac, and Phenix were used in the refinement and the models were built using Coot. The crystallographic data are summarized in Table S3.

EMSA

601 DNA and NCPs were produced as described in (Klein et al., 2016). Increasing amounts of MORC3 His-ATPase domain (1 to 20 molar excess) were incubated with 601 DNA (3 pM) or with NCPs (3 pM) in 20 mM Tris-HCl pH 7.5 buffer, 150 mM NaCl, 2 mM DTT for 1 hour at room temperature. The reaction mixtures were loaded on 5% polyacrylamide gels and electrophoresis was performed in 0.2 x TB buffer at 150 V for 1 hour on ice. Gels were stained with ethidium bromide and visualized with AlphaImager (AlphaInotech).

ATPase assays

The ATPase assays were performed using EnzChek Phosphate Assay Kit (Molecular Probes). The reactions were carried out on 1.5–3.0 μM of MORC3 His-ATPase or His-ATPase-CW, 3 mM ATP, in the presence and absence of 20–40 μg/mL either dsDNA (14mer, GCTTTGCTGTAAGG; Integrated DNA Technologies), 20 μg/mL mono/dinucleosomes (Reaction Biology Corp.) or 1 μM 601 DNA in a buffer containing 50 mM Tris-HCl, pH 7.5, 1 mM $MgCl_2$, 0.1 mM sodium azide, 200 μM MESG, and 1 U of PNP. Reaction mixtures were incubated for 20 mins at 22 °C or 30 mins at 30 °C, and the release of inorganic phosphate was monitored by measuring the absorbance at 360 nm on a Nanodrop 2000c spectrophotometer (Thermo Scientific). In the presence of inorganic phosphate, produced by the hydrolysis of ATP to ADP, MESG is enzymatically converted to ribose 1-phosphate and 2-amino-6-mercapto-7-methylpurine by PNP, resulting in a shift in the wavelength absorbance from 330 nm for MESG to 360 nm for the product. Error was calculated as the standard deviation between at least three separate experiments (two experiments for ATPase-CW with DNA or H3 at 30 °C). Due to the sensitivity to inorganic phosphate, HEPES buffer was used during purification of the proteins for this assay.

Chromatin Association Assays

The cDNA encoding full-length human MORC3 was acquired from the CCSB Human ORFeome Collection, version 5.1 and was cloned as an N-terminal 3xFLAG fusion into pSEB-N3F (generous gift of Dr. Tong-Chuan He, University of Chicago). Amino acid substitutions were introduced by Quick Change site-directed mutagenesis (Strategene). Asynchronously growing HeLa cells were harvested by trypsinization 48 hours post transfection with the indicated FLAG-tagged MORC3 constructs. Pellets were washed once with cold 1x PBS, snap frozen in liquid N_2 and either processed immediately or stored at −80°C. Cell pellets were resuspended in 1 x volume CSK buffer (10 mM PIPES pH 7.0, 300 mM sucrose, 100 mM NaCl, 3 mM $MgCl_2$, 0.1% Triton X-100 and 1x Complete EDTA-Free protease inhibitor cocktail from Roche) and incubated on ice for 20 min. Total protein was quantified by Bradford Assay (BioRad), and 10% of this total fraction was combined with an equivalent volume of CSK buffer supplemented with Universal Nuclease (Thermo, 1:5,000). Note that the concentration of the total fraction is now 0.5x. The remaining cell lysate was centrifuged at 1,300 × g for 5 min at 4°C. The supernatant (soluble fraction) was collected. The chromatin pellet was resuspended in 1x volume CSK buffer and kept on ice for 10 min before being spun again at 1,300 × g for 5 min at 4°C. The supernatant was discarded and the chromatin pellet was solubilized in CSK buffer supplemented with Universal Nuclease. 1–5 μg of protein from each fraction (estimated from Bradford on total extract) was resolved by SDS-PAGE, transferred to PVDF membrane (Thermo), and probed with the indicated antibodies (Flag, Sigma #F1804, 1:5,000; β-tubulin, Millipore #05-661, 1:5,000, H3, Epicypher #13-0001, 1:25,000).

Immunofluorescence

Asynchronously growing HeLa cells were cultured in Nunc Lab-TeK II chamber slides (Thermo) and transiently transfected with 3xFLAG-MORC3 transgenes using TurboFect transfection reagent (Thermo). Cells were washed with 1x PBS 48 hours post transfection and fixed with cold methanol at −20°C for 10 min. Fixed cells were blocked for 30 min in PBS containing 1% (w/v) BSA prior to being labeled with an anti-FLAG antibody (Sigma #F7435, 1:200) in PBS containing 1% BSA for 1 hour at 25°C. Following washing with PBS, cells were incuba ted with an Alexa Fluor 647-conjugated secondary antibody (Life Technologies #A21245, 1:1000) for 1 hour at 25°C protected from light. Cells were washed with PBS and mounted using SlowFade Gold Antifade mountant with DAPI (Thermo). Images were acquired using a Nikon A1+ RSi confocal microscope using a 100X objective following excitation with 403-nm and 6400-nm solid-state lasers.

Supplementary Material

Refer to Web version on PubMed Central for supplementary material.

Acknowledgments

We thank Jovylyn Gatchalian, Sean Bevers and Ruben Rosas Ospina for helping with experiments, Norimitsu Inoue for kindly providing original cDNA of MORC3, Jay Nix at beam line 4.2.2 of the ALS in Berkeley for help with X-ray crystallographic data collection, and University of Colorado Denver Biophysics Core facility. We thank the UNC High Throughput Peptide Synthesis and Array Core Facility for providing modified histone peptides used for microarray fabrication. We also thank the VARI Confocal Microscopy and Quantitative Imaging Core Facility for

assistance with immunofluorescence image acquisition. This work was supported by NIH grants R01 GM106416 and GM100907 to T.G.K, R00 CA181343 to S.B.R., R01 CA117907 to J.M.E., and R01 GM110058 to B.D.S. F.H.A. was supported by the NIH grant T32AA007464 and the AHA postdoctoral fellowship.

References

Dutta R, Inouye M. GHKL, an emergent ATPase/kinase superfamily. Trends in biochemical sciences. 2000; 25:24–28. [PubMed: 10637609]

Fiorentino DF, Chung LS, Christopher-Stine L, Zaba L, Li S, Mammen AL, Rosen A, Casciola-Rosen L. Most patients with cancer-associated dermatomyositis have antibodies to nuclear matrix protein NXP-2 or transcription intermediary factor 1gamma. Arthritis and rheumatism. 2013; 65:2954–2962. [PubMed: 24037894]

Gonzalez-Fernandez R, Morales M, Avila J, Martin-Vasallo P. Changes in leukocyte gene expression profiles induced by antineoplastic chemotherapy. Oncology letters. 2012; 3:1341–1349. [PubMed: 22783446]

Gunawardena H, Wedderburn LR, Chinoy H, Betteridge ZE, North J, Ollier WE, Cooper RG, Oddis CV, Ramanan AV, Davidson JE, et al. Autoantibodies to a 140-kd protein in juvenile dermatomyositis are associated with calcinosis. Arthritis and rheumatism. 2009; 60:1807–1814. [PubMed: 19479859]

Guo X, Wang L, Li J, Ding Z, Xiao J, Yin X, He S, Shi P, Dong L, Li G, et al. Structural insight into autoinhibition and histone H3-induced activation of DNMT3A. Nature. 2015; 517:640–644. [PubMed: 25383530]

Hallam DM, Maroun LE. Anti-gamma interferon can prevent the premature death of trisomy 16 mouse cortical neurons in culture. Neuroscience letters. 1998; 252:17–20. [PubMed: 9756348]

Hauk G, Bowman GD. Structural insights into regulation and action of SWI2/SNF2 ATPases. Current opinion in structural biology. 2011; 21:719–727. [PubMed: 21996440]

Hauk G, McKnight JN, Nodelman IM, Bowman GD. The chromodomains of the Chd1 chromatin remodeler regulate DNA access to the ATPase motor. Molecular cell. 2010; 39:711–723. [PubMed: 20832723]

He F, Umehara T, Saito K, Harada T, Watanabe S, Yabuki T, Kigawa T, Takahashi M, Kuwasako K, Tsuda K, et al. Structural insight into the zinc finger CW domain as a histone modification reader. Structure. 2010; 18:1127–1139. [PubMed: 20826339]

Ichimura Y, Matsushita T, Hamaguchi Y, Kaji K, Hasegawa M, Tanino Y, Inokoshi Y, Kawai K, Kanekura T, Habuchi M, et al. Anti-NXP2 autoantibodies in adult patients with idiopathic inflammatory myopathies: possible association with malignancy. Annals of the rheumatic diseases. 2012; 71:710–713. [PubMed: 22258483]

Kimura Y, Sakai F, Nakano O, Kisaki O, Sugimoto H, Sawamura T, Sadano H, Osumi T. The newly identified human nuclear protein NXP-2 possesses three distinct domains, the nuclear matrix-binding, RNA-binding, and coiled-coil domains. The Journal of biological chemistry. 2002; 277:20611–20617. [PubMed: 11927593]

Klein BJ, Muthurajan UM, Lalonde ME, Gibson MD, Andrews FH, Hepler M, Machida S, Yan K, Kurumizaka H, Poirier MG, et al. Bivalent interaction of the PZP domain of BRPF1 with the nucleosome impacts chromatin dynamics and acetylation. Nucleic acids research. 2016; 44:472–484. [PubMed: 26626149]

Lane AA, Chapuy B, Lin CY, Tivey T, Li H, Townsend EC, van Bodegom D, Day TA, Wu SC, Liu H, et al. Triplication of a 21q22 region contributes to B cell transformation through HMGN1 overexpression and loss of histone H3 Lys27 trimethylation. Nature genetics. 2014; 46:618–623. [PubMed: 24747640]

Law JA, Du J, Hale CJ, Feng S, Krajewski K, Palanca AM, Strahl BD, Patel DJ, Jacobsen SE. Polymerase IV occupancy at RNA-directed DNA methylation sites requires SHH1. Nature. 2013; 498:385–389. [PubMed: 23636332]

Li DQ, Nair SS, Kumar R. The MORC family: new epigenetic regulators of transcription and DNA damage response. Epigenetics. 2013; 8:685–693. [PubMed: 23804034]

Li X, Foley EA, Molloy KR, Li Y, Chait BT, Kapoor TM. Quantitative chemical proteomics approach to identify post-translational modification-mediated protein-protein interactions. Journal of the American Chemical Society. 2012; 134:1982–1985. [PubMed: 22239320]

Ling KH, Hewitt CA, Tan KL, Cheah PS, Vidyadaran S, Lai MI, Lee HC, Simpson K, Hyde L, Pritchard MA, et al. Functional transcriptome analysis of the postnatal brain of the Ts1Cje mouse model for Down syndrome reveals global disruption of interferon-related molecular networks. BMC genomics. 2014; 15:624. [PubMed: 25052193]

Liu Y, Tempel W, Zhang Q, Liang X, Loppnau P, Qin S, Min J. Family-wide characterization of histone binding abilities of human CW domain containing proteins. The Journal of biological chemistry. 2016

Madan V, Chinoy H, Griffiths CE, Cooper RG. Defining cancer risk in dermatomyositis. Part I. Clinical and experimental dermatology. 2009; 34:451–455. [PubMed: 19522981]

Maroun LE, Heffernan TN, Hallam DM. Partial IFN-alpha/beta and IFN-gamma receptor knockout trisomy 16 mouse fetuses show improved growth and cultured neuron viability. Journal of interferon & cytokine research : the official journal of the International Society for Interferon and Cytokine Research. 2000; 20:197–203.

Mimura Y, Takahashi K, Kawata K, Akazawa T, Inoue N. Two-step colocalization of MORC3 with PML nuclear bodies. Journal of cell science. 2010; 123:2014–2024. [PubMed: 20501696]

Moissiard G, Cokus SJ, Cary J, Feng S, Billi AC, Stroud H, Husmann D, Zhan Y, Lajoie BR, McCord RP, et al. MORC family ATPases required for heterochromatin condensation and gene silencing. Science. 2012; 336:1448–1451. [PubMed: 22555433]

Musselman CA, Kutateladze TG. Handpicking epigenetic marks with PHD fingers. Nucleic acids research. 2011; 39:9061–9071. [PubMed: 21813457]

Musselman CA, Lalonde ME, Cote J, Kutateladze TG. Perceiving the epigenetic landscape through histone readers. Nature structural & molecular biology. 2012; 19:1218–1227.

Narlikar GJ, Sundaramoorthy R, Owen-Hughes T. Mechanisms and functions of ATP-dependent chromatin-remodeling enzymes. Cell. 2013; 154:490–503. [PubMed: 23911317]

Pastor WA, Stroud H, Nee K, Liu W, Pezic D, Manakov S, Lee SA, Moissiard G, Zamudio N, Bourc'his D, et al. MORC1 represses transposable elements in the mouse male germline. Nature communications. 2014; 5:5795.

Peña PV, Davrazou F, Shi X, Walter KL, Verkhusha VV, Gozani O, Zhao R, Kutateladze TG. Molecular mechanism of histone H3K4me3 recognition by plant homeodomain of ING2. Nature. 2006; 442:100–103. [PubMed: 16728977]

Rosendorff A, Sakakibara S, Lu S, Kieff E, Xuan Y, DiBacco A, Shi Y, Shi Y, Gill G. NXP-2 association with SUMO-2 depends on lysines required for transcriptional repression. Proceedings of the National Academy of Sciences of the United States of America. 2006; 103:5308–5313. [PubMed: 16567619]

Rothbart SB, Krajewski K, Strahl BD, Fuchs SM. Peptide microarrays to interrogate the "histone code". Methods in enzymology. 2012; 512:107–135. [PubMed: 22910205]

Sullivan KD, Lewis HC, Hill AA, Pandey A, Jackson LP, Cabral JM, Smith KP, Liggett LA, Gomez EB, Galbraith MD, et al. Trisomy 21 consistently activates the interferon response. eLife. 2016; 5

Takahashi K, Yoshida N, Murakami N, Kawata K, Ishizaki H, Tanaka-Okamoto M, Miyoshi J, Zinn AR, Shime H, Inoue N. Dynamic regulation of p53 subnuclear localization and senescence by MORC3. Molecular biology of the cell. 2007; 18:1701–1709. [PubMed: 17332504]

Torres IO, Kuchenbecker KM, Nnadi CI, Fletterick RJ, Kelly MJ, Fujimori DG. Histone demethylase KDM5A is regulated by its reader domain through a positive-feedback mechanism. Nature communications. 2015; 6:6204.

Wang GG, Song J, Wang Z, Dormann HL, Casadio F, Li H, Luo JL, Patel DJ, Allis CD. Haematopoietic malignancies caused by dysregulation of a chromatin-binding PHD finger. Nature. 2009; 459:847–851. [PubMed: 19430464]

Watson AA, Mahajan P, Mertens HD, Deery MJ, Zhang W, Pham P, Du X, Bartke T, Zhang W, Edlich C, et al. The PHD and chromo domains regulate the ATPase activity of the human chromatin remodeler CHD4. Journal of molecular biology. 2012; 422:3–17. [PubMed: 22575888]

Highlights

- MORC3 is upregulated in Down syndrome and is linked to cancer
- MORC3 CW domain binds to methylated histone H3K4
- The CW-H3K4me interaction is essential for MORC3 recruitment to chromatin
- The CW domain negatively regulates MORC3 DNA-dependent ATPase activity

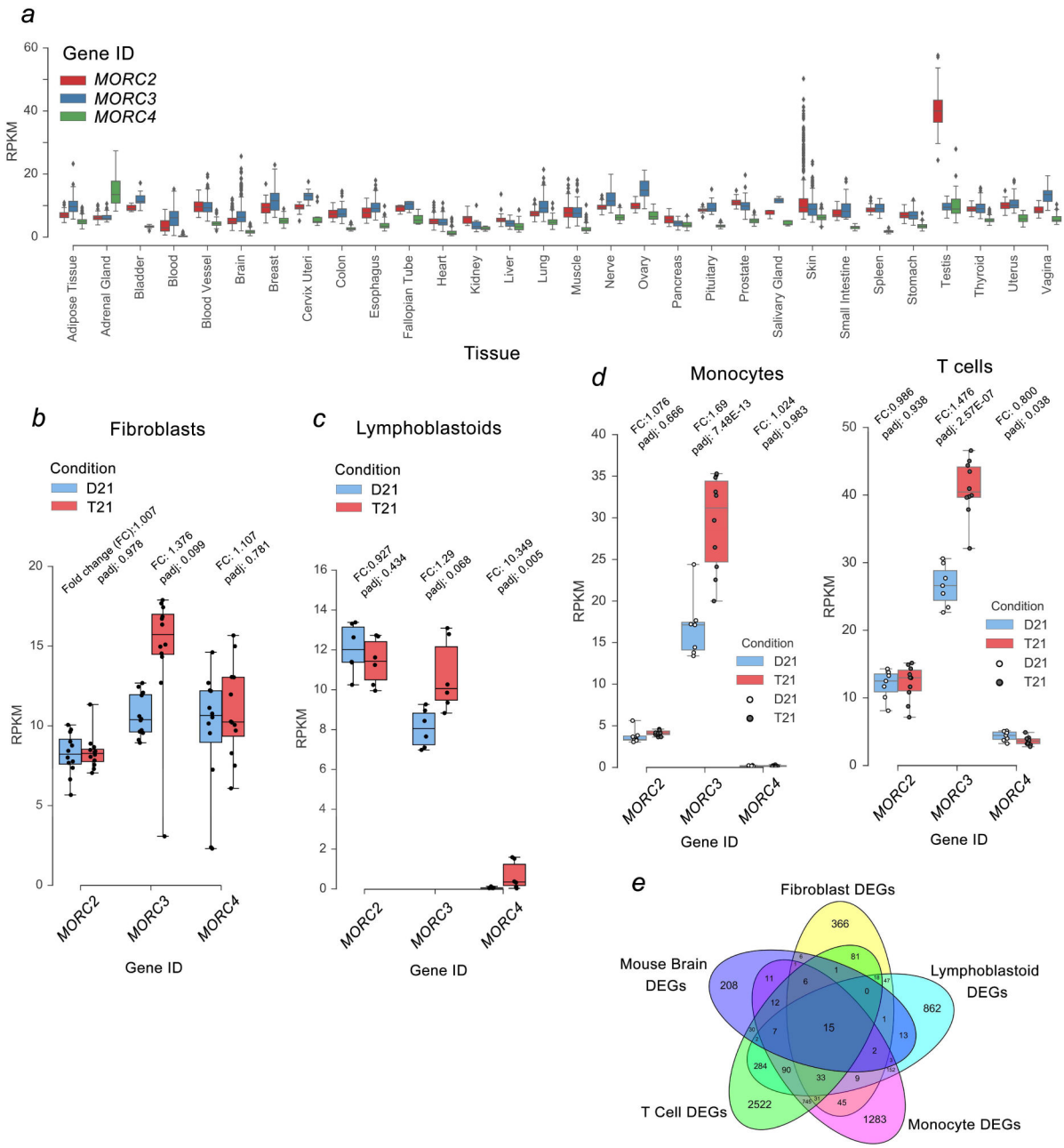

Figure 1. MORC3 is consistently upregulated in Trisomy 21 cells

(*a*) Box and whisker plots of *MORC2*, *MORC3* and *MORC4* expression levels across tissue types from the GTEx Portal. (*b–d*) Box and whisker plots of *MORC3, MORC2* and *MORC4* expression in D21 and T21 fibroblasts (*b*), lymphoblastoid cell lines (*c*), and patient monocytes and T cells (*d*). mRNA expression values are in reads per kilobase per million (RPKM). Benjamini-Hochberg adjusted p-values were calculated using DESeq2. (*e*) Venn diagram of differentially expressed genes in Down syndrome from human fibroblasts, human lymphoblastoids, and mouse brains. See also Figure S1.

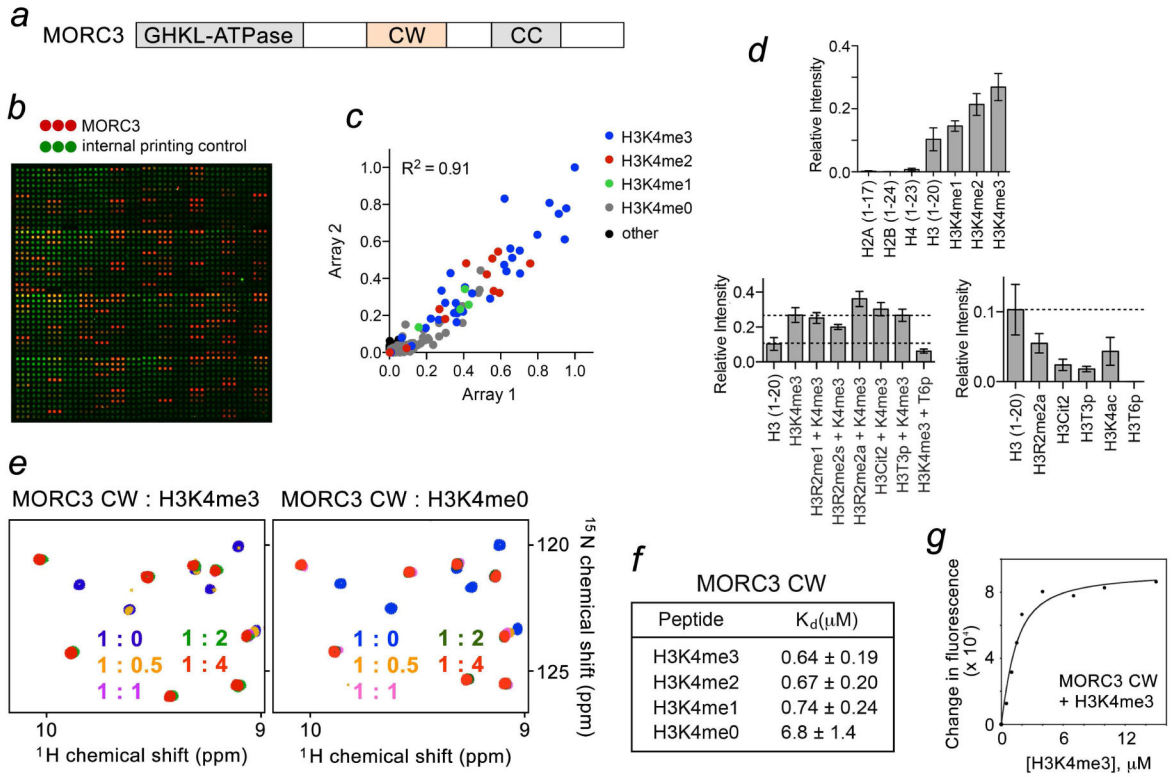

Figure 2. MORC3-CW binds to the histone H3 tail

(*a*) Architecture of MORC3. (*b*) Representative scanned image of a peptide microarray hybridized with GST-MORC3 CW domain. Red spots are bound MORC3. Green spots are an internal printing control and are used to filter false negatives from quantified datasets (see (Rothbart et al., 2012)). (*c*) Scatter plot of relative signal intensities from two microarrays hybridized with GST-MORC3 CW domain. Average signal intensities from quantified arrays were normalized to the most intense series of peptide spots and plotted on a relative scale from 0 (weak binding) to 1 (strong binding). The correlation coefficient was calculated by linear regression analysis using GraphPad Prism v5. (*d*) Normalized average microarray signal intensities measuring the interaction GST-MORC3 CW domain with the indicated histone peptides. Error represents ± s.e.m. from two arrays. (*e*) Superimposed $^{1}H,^{15}N$ HSQC spectra of MORC3-CW collected upon titration with H3K4me3 and H3K4me0 peptides (residues 1–12 of H3). Spectra are color coded according to the protein:peptide molar ratio. (*f*) Binding affinities of wild type MORC-CW for the indicated histone peptides measured by tryptophan fluorescence. (*g*) Representative binding curve used to determine the K_d values by fluorescence. See also Tables S1 and S2.

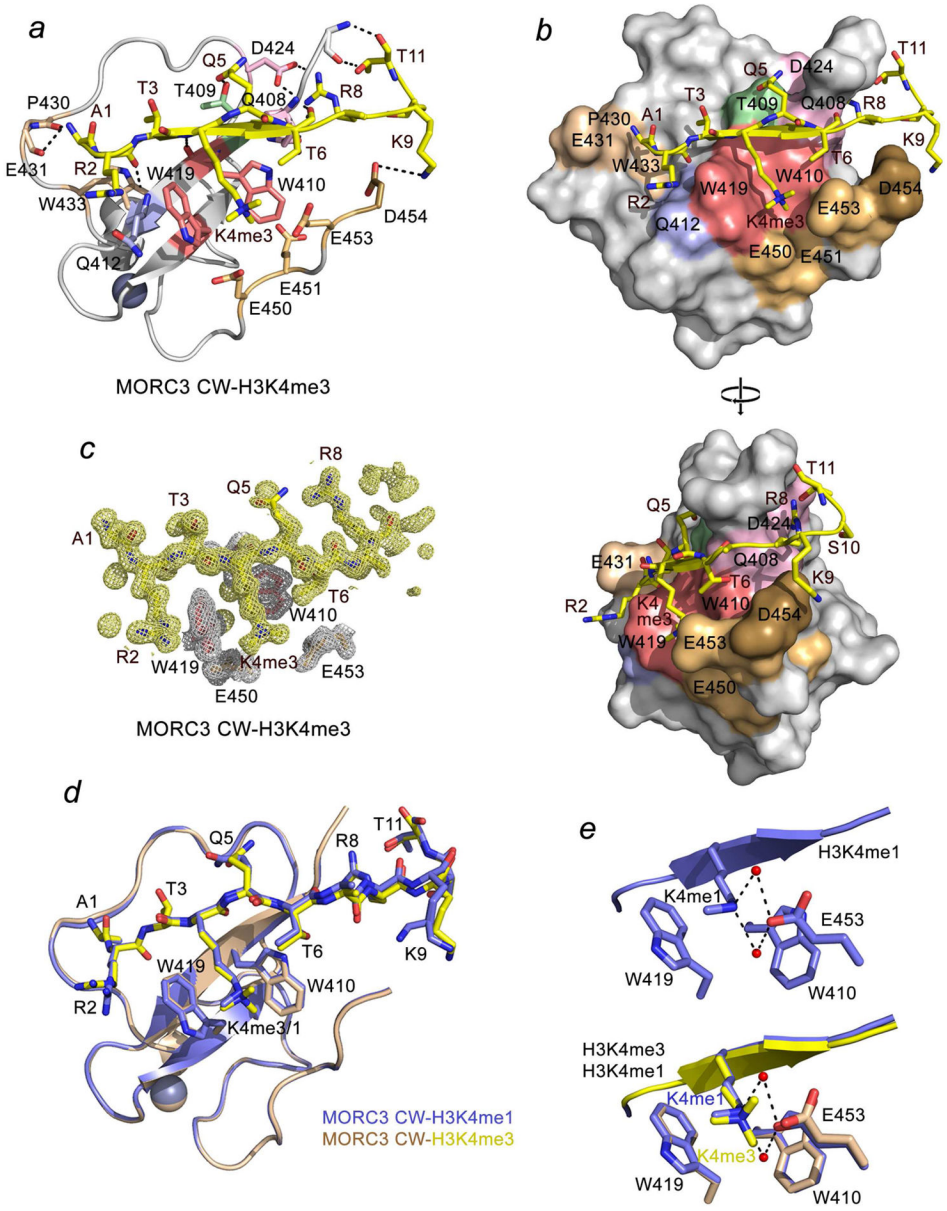

Figure 3. The molecular basis for recognition of H3K4me3 and H3K4me1 by MORC3-CW

(*a*) The ribbon diagram of the MORC3 CW domain in complex with H3K4me3 peptide (yellow). Dashed lines represent intermolecular hydrogen bonds. The protein residues involved in the interactions with A1, R2, K4me3, Q5, R8 and K9 of the peptide are colored wheat, blue, salmon, light green, pink and brown, respectively. (*b*) The surface cartoon of CW domain with histone peptide shown in ribbon and stick. (*c*) A $2F_o{-}F_c$ map was calculated and contoured at 1.0σ as a yellow mesh around the model of histone peptide and grey mesh around Trp-groove residues. (*c*) Overlay of the structures of the MORC3 CW:H3K4me3 and MORC3 CW:H3K4me1 complexes. (*d*) A zoom-in view of the superimposed K4me1- and K4me3-binding grooves. Water molecules are shown as red spheres. See also Table S3.

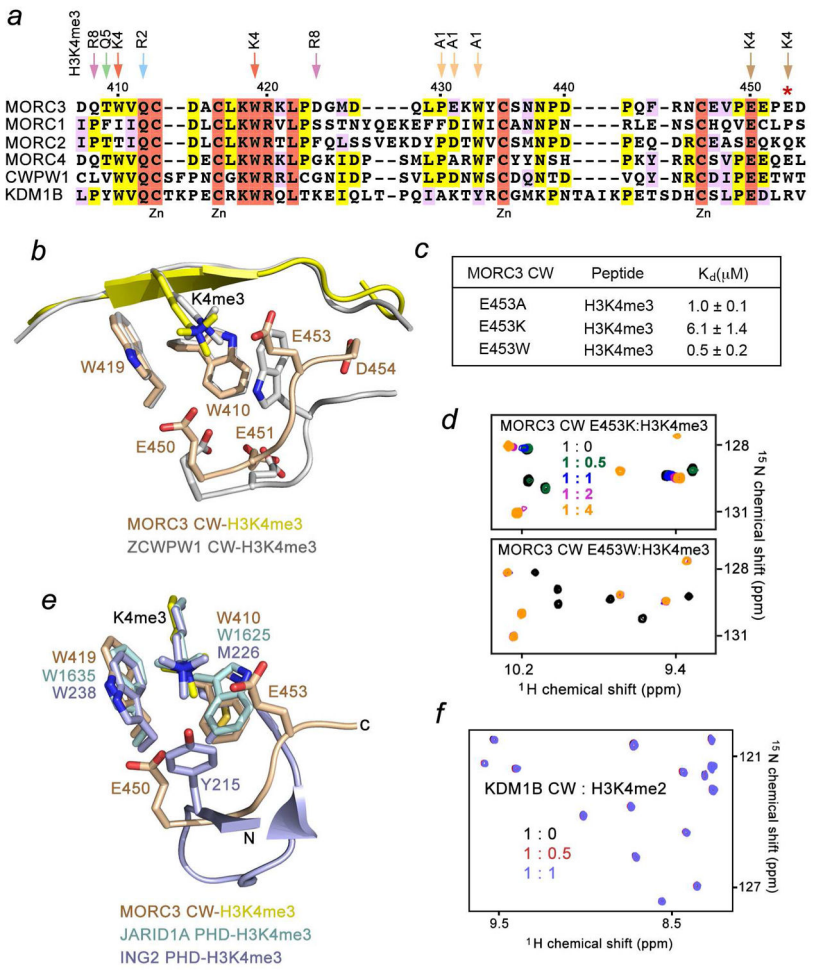

Figure 4. The end-wall residues control selectivity of MORC3-CW

(*a*) Alignment of the CW domain sequences: absolutely, moderately and weakly conserved residues are colored red, yellow and light purple, respectively. The residues of MORC3-CW involved in contact with each residue of histone H3 are indicated by arrows. An asterisk indicates E453. (*b*) A close-up view of the overlaid K4me3-binding sites in MORC3 (wheat) and ZCWPW1 (grey). (*c*) Binding affinities of the MORC3-CW mutants as determined by intrinsic tryptophan fluorescence. (*d*) Superimposed $^{1}H,^{15}N$ HSQC spectra of mutated MORC3-CW, collected upon titration with H3K4me3 peptide. Spectra are color coded according to the protein:peptide molar ratio. (*e*) A close-up view of the overlaid K4me3-binding sites in MORC3-CW (wheat) and PHD fingers of JARID1A (cyan) and ING2 (purple). (*f*) Superimposed $^{1}H,^{15}N$ HSQC spectra of KDM1B CW, recorded as H3K4me2 was titrated in. See also Figure S2.

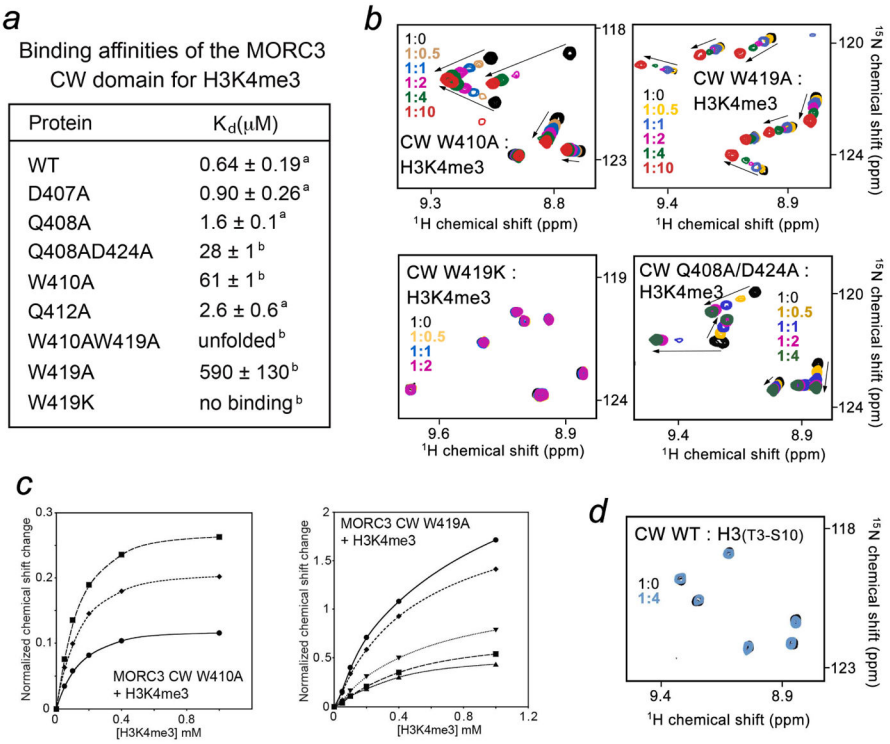

Figure 5. The critical role of the histone-binding site residues of MORC3-CW

(*a*) Binding affinities of the MORC3-CW mutants as determined by tryptophan fluorescence ([a]) or NMR ([b]). (*b*) Superimposed $^{1}H,^{15}N$ HSQC spectra of the MORC3-CW mutants, collected upon titration with H3K4me3. Spectra are color coded according to the protein:peptide molar ratio. (c) Representative binding curves used to determine the K_d values by NMR. (*d*) Superimposed $^{1}H,^{15}N$ HSQC spectra of MORC3-CW, recorded as H3 peptide (residues T3-S10) was titrated in. See also Figures S3 and S4.

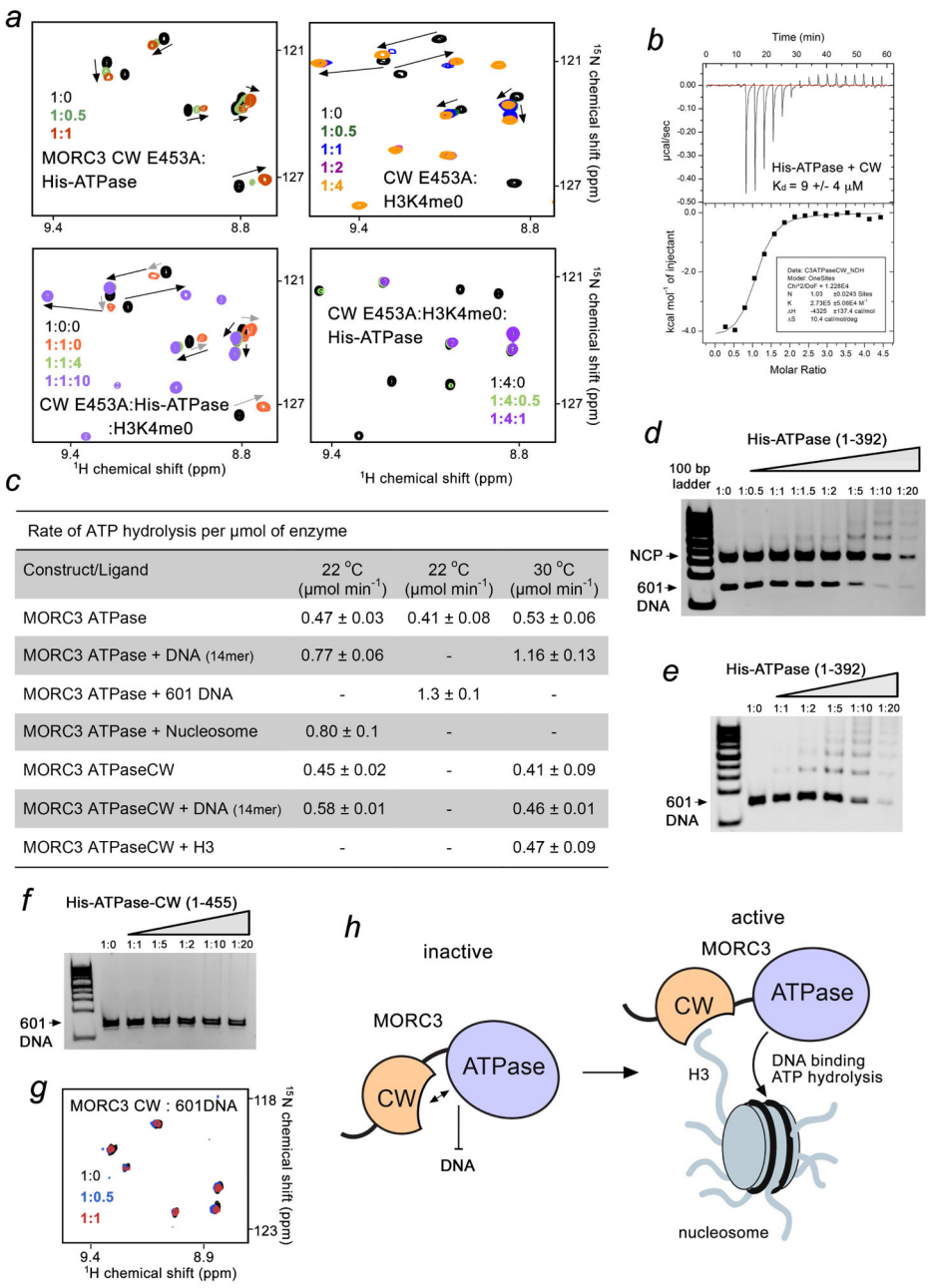

Rate of ATP hydrolysis per µmol of enzyme			
Construct/Ligand	22 °C (µmol min^{-1})	22 °C (µmol min^{-1})	30 °C (µmol min^{-1})
MORC3 ATPase	0.47 ± 0.03	0.41 ± 0.08	0.53 ± 0.06
MORC3 ATPase + DNA (14mer)	0.77 ± 0.06	-	1.16 ± 0.13
MORC3 ATPase + 601 DNA	-	1.3 ± 0.1	-
MORC3 ATPase + Nucleosome	0.80 ± 0.1	-	-
MORC3 ATPaseCW	0.45 ± 0.02	-	0.41 ± 0.09
MORC3 ATPaseCW + DNA (14mer)	0.58 ± 0.01	-	0.46 ± 0.01
MORC3 ATPaseCW + H3	-	-	0.47 ± 0.09

Figure 6. MORC3 is an ATPase

(*a*) Superimposed ^{1}H,^{15}N TROSY (top-left and bottom row) spectra and ^{1}H,^{15}N HSQC spectra (top-right) of MORC3-CW E453A, collected upon titration with indicated ligands. Spectra are color coded according to the protein:ligands molar ratio. (*b*) Representative ITC binding curves observed for the interaction between MORC3 His-ATPase and CW. (*c*) The rate of ATP hydrolysis by MORC3 His-ATPase. Error represents SD between at least three separate experiments (two experiments for His-ATPase-CW with DNA or H3 at 30 °C). (*d, e*) EMSA with NCPs (d) or 601 DNA (e) in the presence of increasing amounts of His-ATPase, as described in methods. (*f*) EMSA with 601 DNA in the presence of increasing

amounts of His-ATPase-CW. (*g*) Superimposed $^{1}H,^{15}N$ HSQC spectra of MORC3-CW upon titration with 601 DNA. (*h*) A model for the regulation of MORC3. See also Figure S5.

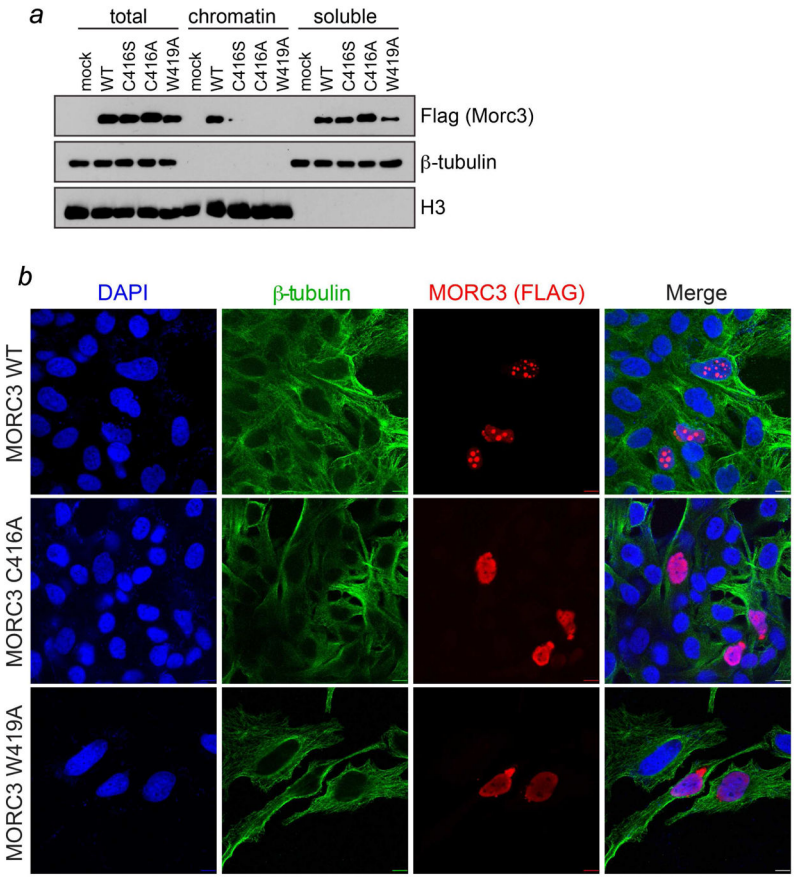

Figure 7. The CW domain is required for the recruitment of MORC3 to chromatin

(*a*) Chromatin association assays for FLAG-tagged MORC3 (WT) or the indicated mutants from asynchronously growing HeLa cells. Mock, no DNA control. (*b*) Representative confocal microscopy images of FLAG-tagged wild-type and mutant forms of MORC3 in HeLa cells. Scale bars, 10 μm. See also Figure S6.